Simultaneous manifestations of the 2D van Hove singularity and the Fermi surface nesting in the acoustic soft phonon mode of β-NiAl alloys

1997 J. Phys.: Condens. Matter 9 10339

(http://iopscience.iop.org/0953-8984/9/47/004)

J. Phys.: Condens. Matter **9** (1997) 10339–10351. Printed in the UK PII: S0953-8984(97)86250-9

Simultaneous manifestations of the 2D van Hove singularity and the Fermi surface nesting in the acoustic soft phonon mode of β-NiAl alloys

I I Naumov and O I Velikokhatniy

Institute of Physics of Strength and Materials Science, 634021, Tomsk, Russia

Received 21 July 1997

Abstract. The experimentally observed composition and uniaxial-stress dependences of the TA_2 soft phonon mode in $\beta-Ni_xAl_{1-x}$ alloy have been interpreted using numerical calculations of the electronic band structure, elastic shear constant C', generalized susceptibility $\chi(\boldsymbol{q})$ and different sections of Fermi surface as a basis. It is shown that the main features of these dependences are attributable to two different band structure peculiarities, namely, to Fermi surface nesting and 2D van Hove singularity in the density of states. Whereas the nesting vector $2\boldsymbol{k}_F$ fixes the position of a dip (Kohn anomaly) in the TA_2 phonon branch, the separation between the Fermi level and the energy of the 2D van Hove singularity governs the softening (hardening) of this branch as a whole.

1. Introduction

Recently the Ni_xAl_{1-x} shape memory alloy system has been the subject of intensive investigations ([1–6] and others). Cooling of the alloys having compositions in the range $0.60 \leqslant x \leqslant 0.64$ induces a $\beta \rightarrow 7R \rightarrow 3R$ chain of structural transformations [1, 3, 4], where β is an initial high-temperature structure of the CsCl type, 7R is a 'sevenfold' intermediate structure and 3R is a low-temperature martensitic structure of the $L1_0$ type. Above the temperature of the onset of the $\beta \rightarrow 7R$ transition there is a whole series of premartensitic anomalies [1] and, particularly, softening of the elastic constant $C' = (C_{11} - C_{12})/2$ associated with the long-wave behaviour of the transverse acoustic vibration mode $[\xi\xi 0]$ TA_2 [7, 8]. Furthermore, C' also softens strongly with increasing Ni concentration, x [7, 8]. The TA_2 phonon mode demonstrates an anomaly at some intermediate wave vector $\boldsymbol{q}_m = (2\pi/a)[\xi_m, \xi_m, 0]$ which depends on the composition x (a is a lattice parameter) [9]. The quantity ξ_m, which characterizes the position of the anomaly, falls rapidly with increasing x; as x increases, for example, from 0.50 to 0.625 it changes from approximately 1/4 to 1/6 respectively (it should be noted that $\xi = 1/2$ corresponds to the boundary of the Brillouin zone (BZ)). Besides, the entire TA_2 curve softens with increasing x.

The neutron scattering experiments on a single crystal of $Ni_{0.625}Al_{0.375}$ [6] revealed the phonon anomaly to show a strong dependence on uniaxial stress applied along the [001] direction as well. Namely, the dip in the TA_2 along $[\pm 1, \pm 1, 0]$ directions (i.e. perpendicularly to the applied stress) deepens and shifts from $\xi_m = 0.14$ to $\xi_m = 0.18$ as one proceeds from zero stress to stress of 85 MPa. Furthermore, the entire TA_2 curve softens with increasing stress.

0953-8984/97/4710339+13$19.50

Shapiro *et al* [9] suggested a hypothesis that the phonon anomaly is of electronic nature and connected with 'nesting areas' of the Fermi surface (FS), separated by vector $2\boldsymbol{k}_F \approx \boldsymbol{q}_m$. To verify this hypothesis Zhao and Harmon [10] within the method of Varma and Weber [11] calculated the phonon dispersion curves of Ni_xAl_{1-x}. They found that the phonon anomaly in TA_2 arises from the strong electron–phonon interaction and its location, q_m, really is close to the nesting vector $2\boldsymbol{k}_F$ spanning extended cylindrical parts of the FS in the seventh band. Moreover, they were able to reproduce the experimentally observed function $q_m(x)$ over the whole range of concentrations x; this result was obtained independently by Naumov *et al* [12] (see also [15]).

The main aims of this paper are (1) to present new evidence that the dip in the TA_2 phonon branch is of the Kohn type and (2) to show that in addition to parallel flat segments of the Fermi surface there is another electronic peculiarity, which strongly affects the TA_2 phonon branch as well—the 2D van Hove singularity in the density of states $n(\varepsilon)$. As the separation $\eta = \varepsilon_F - \varepsilon_C$ between the Fermi level and the energy of the 2D van Hove singularity ε_C decreases the TA_2 phonon mode softens as a whole. At the same time the nesting vector $2\boldsymbol{k}_F$ spanning two flat pieces of FS controls the position of the Kohn anomaly, $\boldsymbol{q}_m$. To attain this the observed composition and uniaxial-stress dependences of the TA_2 phonon branch are analysed in detail. Keeping in mind that the TA_2 dispersion curve correlates well [10, 12] with the generalized susceptibility for a non-interacting electronic system $\chi(\boldsymbol{q})$ (in particular, the dip in TA_2 precisely corresponding to a maximum in $\chi(\boldsymbol{q})$), we calculate only $\chi(\boldsymbol{q})$, rather than the TA_2 dispersion curve itself. At the same time we calculate the band structure energy contribution to the elastic constant C', which is directly related to TA_2 in the limit of long wavelengths ($q \to 0$).

The paper is organized as follows. In section 2 the details of the numerical calculations are presented. In section 3 we calculate the band structure energy contribution to the elastic shear constants C' for various compositions x; the physical origin of softening of C' with increasing x is discussed. In section 4 the responses of the nesting vector $2\boldsymbol{k}_F$ and generalized susceptibility $\chi(\boldsymbol{q})$ to the composition are analysed and compared with the observed composition dependence of TA_2. In section 5 the transformations of the band structure and $\chi(\boldsymbol{q})$ caused by uniaxial squeezing of the $Ni_{0.625}Al_{0.375}$ crystal are considered and compared with the corresponding transformation of TA_2. Finally, in section 6 we (1) summarize our conclusions about the connection between the peculiarities of the electronic structure and behaviour of the phonon mode under discussion and (2) discuss the 2D van Hove singularity effects in a phonon spectrum as compared with 3D ones.

2. Computational details

To calculate the band structure, elastic constant C' and generalized susceptibility $\chi(\boldsymbol{q})$ the standard linear muffin-tin method (LMTO) with so-called combined correction terms has been used [13]. The local-density approximation as formulated by Barth and Hedin [14] was employed to account for the exchange and correlation. The LMTO basis included 3d, 4s and 4p functions for Ni and 3s, 3p and 3d functions for Al. Similar to [10], [12] and [15] we used a rigid-band model, treating the electron energy spectrum $\varepsilon_\lambda(\boldsymbol{k})$ of the partially disordered alloy Ni_xAl_{1-x} as that of totally ordered $Ni_{0.50}Al_{0.50}$; the substitution of the Ni for Al is supposed to lead only to a change in the number of conduction electrons $Z(x)$ and thus in the Fermi level ε_F. The function $Z(x)$, as in [10], [12] and [15], was chosen by recognizing the fact that each Ni atom maintains a d occupation close to 9.0, so that every 'excess' (relative to the 50–50 alloy) Ni atom brings a single electron to the rigid bands. This gives $Z(x) = 13 - (x - 1/2)(6 - 1)$ and the Fermi level ε_F is lowered as the

x increases. Note that the rigid-band model with the chosen form of $Z(x)$ describes well the concentration dependences of the optical spectra [15] and the phonon anomaly in the TA_2; KKR–CPA calculations also are consistent with the model used (see [10]). This points to the validity of the model and the fact that in the Ni_xAl_{1-x} alloys the 'concentrational' smearing of Fermi surface does not prevent its showing up in physical characteristics.

The band structure energy contribution to the elastic shear constant C' is calculated similarly to that in [16] and [17] from the formula

$$C' = \frac{3}{4}\sum_{\lambda}\left[\int \frac{\partial^2\varepsilon_\lambda(\boldsymbol{k})}{\partial\gamma^2}\theta(\varepsilon_\lambda(\boldsymbol{k})-\varepsilon_F)\,\mathrm{d}\boldsymbol{k} - \int\left(\frac{\partial\varepsilon_\lambda(\boldsymbol{k})}{\partial\gamma}\right)^2\delta(\varepsilon_\lambda(\boldsymbol{k})-\varepsilon_F)\,\mathrm{d}\boldsymbol{k}\right] \tag{1}$$

where γ is the parameter setting the strain matrix $\hat{\varepsilon}$:

$$\hat{\varepsilon} = \begin{pmatrix} (1+\gamma)^{1/3} & 0 & 0 \\ 0 & (1+\gamma)^{1/3} & 0 \\ 0 & 0 & (1+\gamma)^{-2/3} \end{pmatrix}. \tag{2}$$

According to this matrix the integration over $\boldsymbol{k}$ in (1) is performed in the irreducible part (1/16) of the tetragonal BZ and 1276 reference $\boldsymbol{k}$-points are used in this part.

In the calculations we have not dealt with the uniaxial stress, as such. We merely accounted for the stress through the tetragonal distortion $\Delta = (1-c/a)$ (c/a is the tetragonal ratio), taking into consideration that in experiment [6] Δ ranged up to 0.021. Since in the experiment the lattice was strained with hardly any volume change ($\varepsilon_{zz} = -\frac{1}{2}\varepsilon_{xx}$, $\varepsilon_{xx} = \varepsilon_{yy}$), all the calculations at different Δ have been performed under constraint that the atomic volume $\Omega = a^2c/2 =$ constant. The lattice constant a corresponding to $x = 0.5$ and $\Delta = 0$ was taken to be 5.442 [8].

The generalized susceptibility of non-interacting electrons,

$$\chi(\boldsymbol{q}) = \frac{2\Omega}{(2\pi)^3}\int \mathrm{d}\boldsymbol{k}\sum_{\lambda,\lambda'}\frac{\boldsymbol{f}(\varepsilon_\lambda(\boldsymbol{k}))[1-\boldsymbol{f}(\varepsilon_{\lambda'}(\boldsymbol{k}+\boldsymbol{q}))]}{\varepsilon_{\lambda'}(\boldsymbol{k}+\boldsymbol{q})-\varepsilon_\lambda(\boldsymbol{k})} \tag{3}$$

is calculated using the highly precise analytic tetrahedron method [18]; to reach high precision the irreducible (1/48 in the case of a cubic and 1/16 in the case of a tetragonal lattice) part of the BZ is divided into 3375 and 10 125 tetrahedra, correspondingly.

3. x-dependence of C'

Let us consider first the energy band structure of the alloy $Ni_{0.50}Al_{0.50}$ containing 13 valence electrons per unit cell (figure 1). Five initial bands are filled, with the sixth and seventh bands being partially occupied. The band structure is characterized by a wide s–p energy band of Al, which is intersected by a narrow d band, associated with Ni and located $\approx$2 eV below ε_F. Above the Fermi level ε_F and below the d band the $\varepsilon_\lambda(\boldsymbol{k})$ curves have the characteristic form of almost-free electrons, but slightly below ε_F they become significantly flatter because of mixing of the d (e_g) states of Ni with the p states of Al. As a result, on their way, moving from the X to the M and R points shown in figure 2 band 7 practically has no energy dispersion, which leads to a small but sharp peak in the density of the electron states $n(\varepsilon)$ at the energy ε_X located slightly (by $\approx$0.6 eV) below ε_F. All the other factors being the same, this peak would be an ordinary 3D van Hove singularity, but the lack of electronic dispersion turns it into the 2D one.

In view of its importance one needs to consider this question in more detail. The XR and XM lines are those of intersection of two symmetry planes, so that the transverse electron velocity $\boldsymbol{V}_\perp(\boldsymbol{k}) = (\boldsymbol{n}\times\nabla\varepsilon(\boldsymbol{k}))$ equals zero along them ($\boldsymbol{n}$ is the unit vector tangent to the

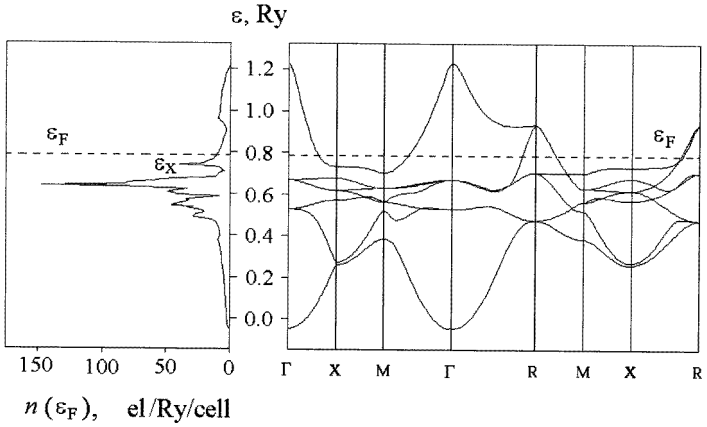

Figure 1. Electronic band structure and density of states of the alloy $Ni_{0.50}Al_{0.50}$.

lines). In this connection the dispersion curves (their parts) of the seventh band along XR and XM can be represented in the form [17]

$$\varepsilon(\boldsymbol{k}) = \varepsilon_1(k_1) + \frac{k_2^2}{2m_2(k_1)} + \frac{k_3^2}{2m_3(k_1)} \tag{4}$$

$$\varepsilon_1(k_1) = \varepsilon_X + \beta(k_1) \tag{5}$$

$k_x \leqslant k_1 \leqslant k_B$, $\beta = \varepsilon_B - \varepsilon_x$, $|\beta| \ll W$ (W is the band width). As $\beta \to 0$, the singular contribution to $n(\varepsilon)$ takes the form

$$\delta n(\varepsilon) \propto \begin{cases} \theta(\varepsilon - \varepsilon_X)\,\mathrm{sign}(m_2(\boldsymbol{k})) & m_2 m_3 > 0 \\ \ln|\varepsilon - \varepsilon_X| & m_2 m_3 < 0. \end{cases} \tag{6}$$

As the analysis shows, along XM $m_2 m_3 > 0$ and $\delta n(\varepsilon)$ is proportional to $\theta(\varepsilon - \varepsilon_X)$, but along XR $m_2 m_3 < 0$ and $\delta n(\varepsilon) \sim \ln|\varepsilon - \varepsilon_X|$, i.e. it is more singular as compared with the first case. In any case the 2D singularity in $n(\varepsilon)$ given by (6) is stronger than the usual 3D one proportional to $[\pm\eta\theta(\pm\eta)]^{1/2}$ ($\eta = \varepsilon - \varepsilon_X$, $\theta(x) = 1$ for $x > 0$, and $\theta(x) = 0$ for $x < 0$).

The calculated band structure energy contribution to the elastic shear constant C' and density of states at the Fermi level $n(\varepsilon_F)$ are plotted versus concentration in figure 3. It is easy to see that the Fermi level ε_F passes through a 2D van Hove singularity in $n(\varepsilon)$ at $x = 0.632$, which corresponds to the change in topology of the FS in the seventh band, namely, to breaking its coherency along the [100]-type directions. At this concentration C' has a sharp minimum due to the second term in (1) which is directly related to $n(\varepsilon_F)$. So, upon going from $x = 0.50$ to $x = 0.632$ the constant C' softens considerably which is consistent with experiments: over this x-interval C' is lowered by a factor of 2.2 [7] or even of 14 [8] (if the x-dependence of C' is extrapolated above $x = 0.605$).

The fact that the proximity of Fermi level to the 2D van Hove point ε_X noticeably manifests itself in the elastic constant C' and, consequently, in the long-wave part of the TA_2 curve is quite natural and is in conformity with a great number of works in which the influence of 3D van Hove points on elastic constants has been investigated (e.g. [15] and [19]). The most surprising fact in our case of 2D singularity, however, is that it affects significantly the entire TA_2 dispersion curve (see sections 4 and 5).

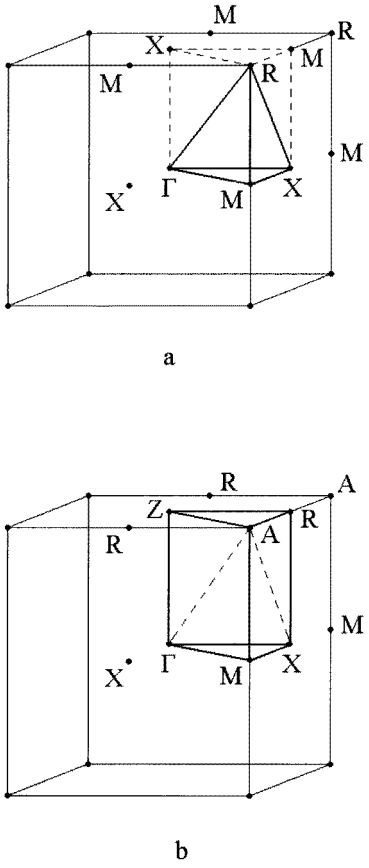

Figure 2. Brillouin zones of the cubic, CsCl (a) and tetragonal (b) structures.

4. x-dependence of $\chi(q)$

The susceptibilities $\chi(q)$ ($q \parallel [110]$) calculated for various x are shown in figure 4(a). In the case of the stoichiometric alloy ($x = 0.50$) the function $\chi(q)$ has a broad maximum at $\xi = 1/4$. However, as x increases this maximum becomes higher and narrower and its position shifts toward lower values of ξ; for example, at $x = 0.60$ it already corresponds to $\xi = 1/7$.

The analysis of the partial contributions shows that the singularity of $\chi(q)$ under discussion is due to $7 \rightarrow 7$ electron transitions, or, in other words, due to the nesting properties of the FS in the seventh band (intraband nesting). The nesting vectors $2k_F$ together with sections of the Fermi surface in the seventh band are shown in figure 5 for the alloys with $x = 0.50$ and $x = 0.60$. With their centres on XM lines they span extended cylindrical parts of the Fermi surface, the generators of which can be seen in the planes with $k_z = \pm 0.3(2\pi/a)$ (figure 5(a,c)) and whose radii are in the plane with $k_x + k_y = 0.5(2\pi/a)$ (figure 5(b,d)). With increasing x from 0.50 to 0.60 the radii of cylindrical parts increase, narrowing the peak of $\chi(q)$. The vector $2k_F$ then decreases because of reduction in the number of occupied states in the seventh band. As x increases the whole curve $\chi(q)$ is shifted upwards (figure 4(a)) and this fact is not due to flat pieces of FS separated

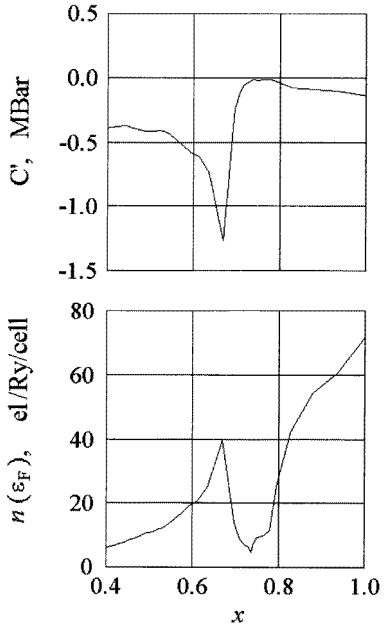

Figure 3. Band structure contribution to the elastic constant C' and density of states at the Fermi level against the concentration of Ni.

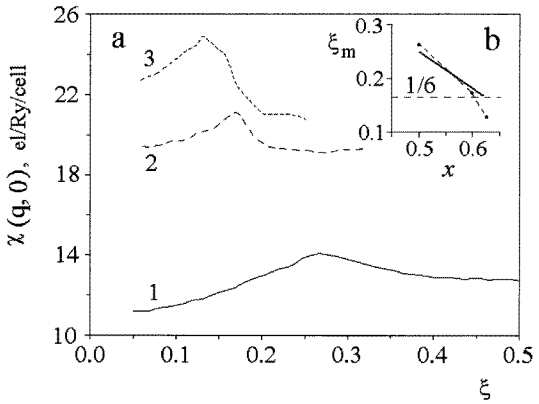

Figure 4. (a) Generalized electron susceptibility $\chi(\boldsymbol{q})$ of the Ni_xAl_{1-x} alloys with $x = 0.50$ (1), 0.60 (2) and 0.625 (3); (b) experimental x-dependence of the soft vectors $\boldsymbol{q}_m$ (continuous curve, according to [9]) and calculated dependence of the nesting vectors $2\boldsymbol{k}_F(x)$ (dashed line).

by the constant wave vector $2\boldsymbol{k}_F$. The growing of the $\chi(\boldsymbol{q})$ as a whole is caused by intraband ($7 \rightarrow 7$) electron transition within the thin $\boldsymbol{k}$-layers adjacent to the BZ faces with $\boldsymbol{k}_z = \pm\pi/a(0\,0\,1)$ having the X point at their centres. Along these layers (especially along the lines close to XR) the seventh band, as noted above, has very little energy dispersion in the vicinity of ε_F. In such a case the approximation $\varepsilon_\lambda(\boldsymbol{k}) - \varepsilon_\lambda(\boldsymbol{k}+\boldsymbol{q}) \approx \boldsymbol{V}_\lambda(\boldsymbol{k}) \cdot \boldsymbol{q}$ is valid over a wide range of $\boldsymbol{q}$, and, according to (3), $\chi(\boldsymbol{q}) \sim 1/(\boldsymbol{V}_\lambda(\boldsymbol{k}) \cdot \boldsymbol{q})$, that is, it becomes higher, as the electron velocity $\boldsymbol{V}_\lambda(\boldsymbol{k}) \equiv \nabla\varepsilon_\lambda(\boldsymbol{k})$ tends to zero. This explains why the entire

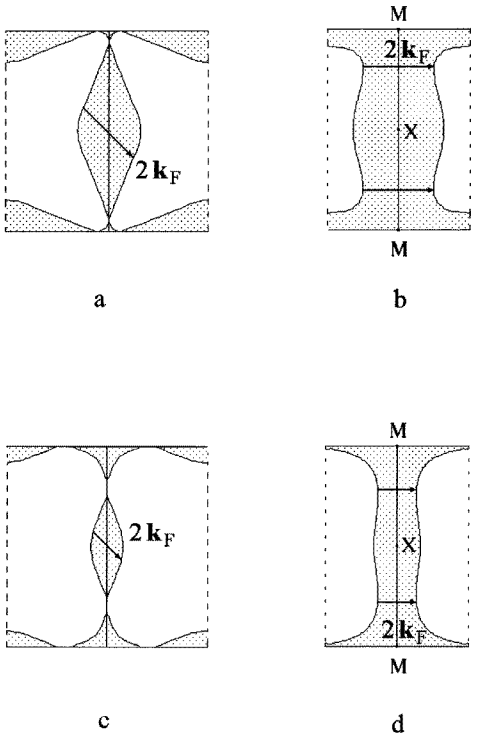

Figure 5. Fragments of the Fermi surface sections in Ni_xAl_{1-x} alloys with $x = 0.50$ (a, b) and $x = 0.60$ (c, d); (a, c) sections in the planes $k_z = \pm 0.3(2\pi/a)$; (b, d) $k_x + k_y = 0.5(2\pi/a)$ planes.

$\chi(\boldsymbol{q})$ curve grows with x until the Fermi level ε_F passes the 2D singularity (or near to this moment).

There is good reason to think that the 2D van Hove point ε_X reveals itself in the TA$_2$ phonon branch mainly through the screening of the valence electron via $\chi(\boldsymbol{q})$ rather than through electron–phonon matrix coupling. Indeed, according to Varma and Weber [11], the critical contribution $\delta\omega^2(\boldsymbol{q})$ to the frequency squared $\omega^2(\boldsymbol{q})$ approximately can be written as follows:

$$\delta\omega^2(\boldsymbol{q}) \propto -\frac{2\Omega}{(2\pi)^3}\int \mathrm{d}^3\boldsymbol{k}|\boldsymbol{V}_\lambda^\perp(\boldsymbol{k}) - \boldsymbol{V}_\lambda^\perp(\boldsymbol{k}+\boldsymbol{q})|^2\frac{\boldsymbol{f}(\varepsilon_\lambda(\boldsymbol{k}))[1-\boldsymbol{f}(\varepsilon_\lambda(\boldsymbol{k}+\boldsymbol{q}))]}{\varepsilon_\lambda(\boldsymbol{k}+\boldsymbol{q}) - \varepsilon_\lambda(\boldsymbol{k})} \tag{7}$$

where $\lambda = 7$ and $\boldsymbol{V}_\lambda^\perp(\boldsymbol{k})$ is a projection of the velocity $\boldsymbol{\nabla}\varepsilon_\lambda(\boldsymbol{k})$ on the axis orthogonal to $\boldsymbol{q}$. Since the seventh band in the vicinity of ε_X is almost dispersionless $\boldsymbol{V}_\lambda^\perp(k) \approx \boldsymbol{V}_\lambda^\perp(k+q) \approx 0$ and the electron–phonon coupling matrix element $g_{k,k+q}^{\lambda\lambda} \sim |\boldsymbol{V}_\lambda^\perp(k) - \boldsymbol{V}_\lambda^\perp(k+q)|^2 \approx 0$. If we take this small matrix element simply to be constant, then $\delta\omega^2(\boldsymbol{q})$ reduces to the formula of $\chi(\boldsymbol{q})$ (3). So, the 2D van Hove singularity should show up in $\omega^2(\boldsymbol{q})$ predominantly through $\chi(\boldsymbol{q})$. If this were so, the frequency $\omega(\boldsymbol{q})$ would soften with increasing $\chi(\boldsymbol{q})$. Such a correlation does take place: the entire $\chi(\boldsymbol{q})$ curve elevates, whereas the entire TA$_2$ dispersion curve drops with x [9]. In the limit of long wavelengths ($q \to 0$) this correlation has already been discussed in the previous sections; indeed, as $\boldsymbol{q}$ tends to zero, $\chi(\boldsymbol{q}) \to n(\varepsilon_F)$ and $\rho\omega^2(q)/q^2 \to C'$ (ρ is the density).

It is evident from figure 4(b) that the dependence of the nesting vectors $2\boldsymbol{k}_F(x)$ is close to the corresponding dependence of the 'soft-mode' wave vectors $\boldsymbol{q}_m(x)$ of TA_2. It is such a correlation that allowed the authors of [10], [12] and [15] to treat the anomaly in TA_2 as of the Kohn type and relate it to the diameters $2\boldsymbol{k}_F$. It is worth noting that, in parallel with the nesting itself, strong electron–phonon interactions, as shown by Zhao and Harmon [10], also favour the formation of a dip in TA_2.

5. Uniaxial-stress dependence of $\chi(\boldsymbol{q})$

Prior to discussing the results of numerical calculations, let us consider some pure geometric aspects of the problem. Under the influence of tetragonal distortion Δ the initial (in a cubic lattice) highly symmetrical [110]-type directions become non-equivalent and break into two groups. Four directions of the first group $[\pm 1, \pm 1, 0]$ lie in the planes, perpendicular to the extension direction [001], and eight directions of the second group ($[\pm 1, 0, \pm a/c]$ and $[0, \pm 1, \pm a/c]$) have a projection on this axis. In the case of no strain ($\Delta = 0$) the nesting vector $2\boldsymbol{k}_F$ is centred, as already noted, on the line XM, at the point situated approximately between the points X and M. In going from a cubic ($\Delta = 0$) to a tetragonal lattice ($\Delta \neq 0$) the XM line must be related to the three lines XM, ZR and XR (figure 2). Consequently, in the distorted crystal the original nesting vector $2\boldsymbol{k}_F$ must be split into three centred on the mentioned lines. It can be easily shown that only the vectors $2\boldsymbol{k}_F$ centred on the XR-type lines can be parallel to the first, [110]-type directions (figure 2). At the same time only the vectors $2\boldsymbol{k}_F$ centred on the ZR- and XM-type lines can be parallel to the second, $[0, \pm 1, \pm a/c]$- and $[\pm 1, 0, \pm a/c]$-type directions, so that along these directions the initial vector $2\boldsymbol{k}_F$ must be split into two.

The Δ-dependence of the maximum in $\chi(\boldsymbol{q})$ along the [110]-direction in the $Ni_{0.625}Al_{0.375}$ alloy is shown in figure 6. One can see that the maximum in $\chi(\boldsymbol{q})$ shifts in the direction of higher wave vectors $\boldsymbol{q}$. The entire curve shows rather an interesting behaviour: at light loads it moves up; however, beginning with $\Delta \approx 0.03$, it starts shifting down dramatically. Along the direction of the second type ($[0, 1, a/c]$, figure 7) $\chi(\boldsymbol{q})$ behaves quite differently: the maximum of $\chi(\boldsymbol{q})$ shifts to the left and the entire curve shifts down (exclusive of the region of small $\boldsymbol{q}$, where $\chi(\boldsymbol{q})$ increases until Δ is, again as high as 0.03).

As analysis shows, the moving of the maximum in $\chi(\boldsymbol{q})$ in opposite directions for $\boldsymbol{q} \parallel [1, 1, 0]$ and $\boldsymbol{q} \parallel [0, 1, a/c]$ arises from the increasing and decreasing of the nesting vectors $2\boldsymbol{k}_F$ (in magnitude), centred on the XR and ZR lines correspondingly (figure 8). With increasing Δ the energy at the X point, as evident from figure 9, drops, but that at the point Z mounts relative to the ε_F, so that the $2\boldsymbol{k}_F \parallel [1, 1, 0]$ elongates and the $2\boldsymbol{k}_F \parallel [0, 1, a/c]$ contracts; in doing so the former correlates with the dip in the TA_2 [110] phonon curve [6] (figure 6(b)).

As previously mentioned, in actuality there must be two nesting vectors parallel to the $[0, 1, a/c]$ direction. This is true (figure 8(d)), but the nesting with $2\boldsymbol{k}_F$ centred on the XM line does not show itself noticeably in $\chi(\boldsymbol{q})$—it leads only to a weak maximum shown in figure 7. The nesting corresponding to $2\boldsymbol{k}_F$ with its centre on the ZR line shows up more strongly due to expanding of the nested areas with Δ (figure 8(c, d)) and involving the electronic states which are closer to the critical energy ε_z (see below).

The Δ-dependences of $\chi(\boldsymbol{q})$ as a whole, again, are caused by the proximity of ε_F to the 2D van Hove singularity. The transformation of the density of states in the $Ni_{0.625}Al_{0.375}$ alloy as the tetragonal deformation Δ increases is shown in figure 10. It is seen that an initial 2D van Hove peak splits into two, the first of which moves away from ε_F, but the

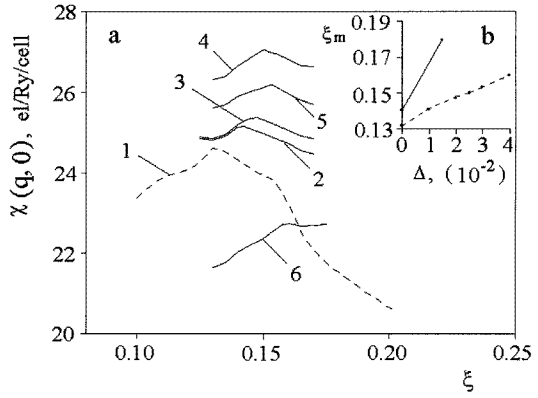

Figure 6. (a) Generalized electron susceptibility $\chi(\boldsymbol{q})$ along [110] in $Ni_{0.625}Al_{0.375}$ for $\Delta = 0.0$ (1), 0.01 (2), 0.02 (3), 0.025 (4), 0.03 (5) and 0.04 (6); (b) experimental Δ-dependence of the soft vectors $\boldsymbol{q}_m$ (continuous curve, according to [6]) and calculated dependence of the nesting vectors $2\boldsymbol{k}_F$ (dashed line).

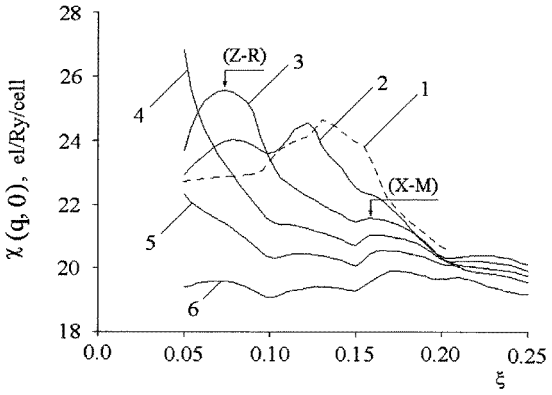

Figure 7. The same as in figure 6, but along $[0, 1, a/c]$. Arrows point to the maxima connected with the nesting vectors $2\boldsymbol{k}_F$, centred on the ZR and XM lines.

second approaches and then passes through it at $\Delta \approx 0.025$. This moment is very close to that when the whole $\chi(\boldsymbol{q})$ ($\boldsymbol{q} \parallel [110]$) reaches the highest position ($\Delta \approx 0.03$). Let us consider this correlation in more detail.

In the original cubic lattice, as mentioned above, the 2D van Hove peak comes from the $\boldsymbol{k}$-lines with $\boldsymbol{V}_\lambda(\boldsymbol{k}) \approx 0$ in the vicinity of ε_X, i.e. from the XM and XR lines located on the faces of BZ. In the tetragonal lattice the $\boldsymbol{k}$-lines with nearly constant energy $\varepsilon_\lambda(\boldsymbol{k})$ still remain; namely, they are along the directions ZR, ZA, XR and XM. In this case $n(\varepsilon)$ passes through the 2D van Hove singularities as ε_F goes through the ε_z or ε_x energies; this explains why the initial van Hove peak splits into two (figure 10). As Δ increases one of the 2D van Hove energies, ε_z, approaches ε_F, but other, ε_x, moves away from it. So, the thin $\boldsymbol{k}$-layers with $\boldsymbol{V}_\lambda(\boldsymbol{k}) \approx 0$ and $\varepsilon_\lambda(k) \approx \varepsilon_F$ appear; these layers adjoin the BZ faces with $k_z = \pm\pi/a(0, 0, a/c)$ and contain the Z points. The electronic transitions $7 \rightarrow 7$ within these $\boldsymbol{k}$-layers give contributions only to $\chi(\boldsymbol{q})$ along the [110], rather than along the $[0, 1, c/a]$ and $[1, 0, c/a]$ directions. This explains why the whole $\chi(\boldsymbol{q})$ curve

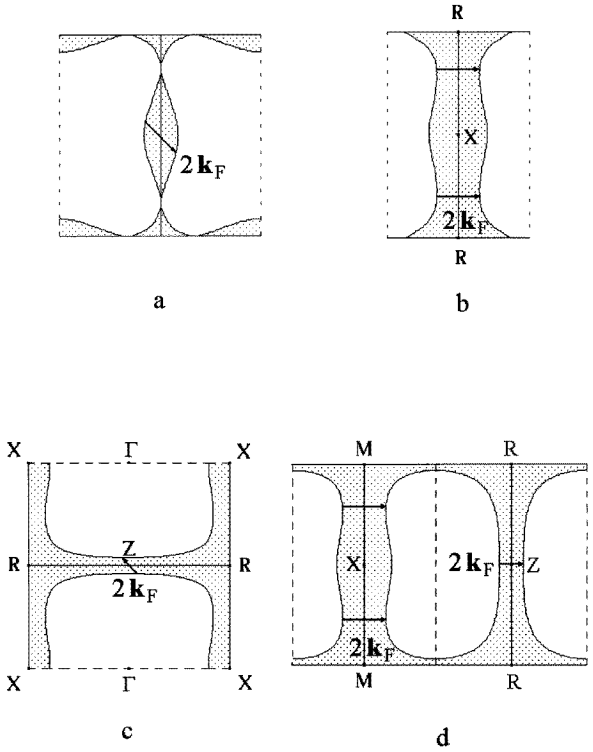

Figure 8. Fragments of the Fermi surface sections in $Ni_{0.625}Al_{0.375}$ alloy with $\Delta = 0.025$ (a, b) and $\Delta = 0.020$ (c, d); (a) sections in the planes $k_z = \pm 0.3(2\pi/c)$; (b, d) $k_x + k_y = 0.5(2\pi/a)$ planes; (c) $k_x = 0$ planes.

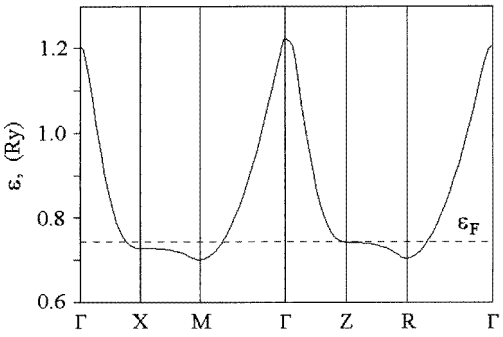

Figure 9. Seventh electronic band in $Ni_{0.625}Al_{0.375}$ under $\Delta = 0.025$.

($\boldsymbol{q} \parallel [110]$) grows with increasing Δ until $\Delta \cong 0.03$. Once Δ has reached the value $\cong 0.03$, the crucial $\boldsymbol{k}$-layers with $\boldsymbol{V}_\lambda(\boldsymbol{k}) \approx 0$ disappear and the entire $\chi(\boldsymbol{q})$ curve falls. Note that in the case of $\boldsymbol{q} \parallel [0, 1, c/a]$ (or $[1, 0, c/a]$) $\chi(\boldsymbol{q})$ correlated with $n(\varepsilon_F)$ only for long wavelengths ($\boldsymbol{q} \approx 0$); that is trivial: $\chi(0)$ is simply $n(\varepsilon_F)$. For 'large' q ($q \geqslant 0.1(2\pi/a)$) $\chi(\boldsymbol{q})$ correlates with the separation between the Fermi level ε_F and the energy of the van Hove singularity ε_x (not ε_z!) and, therefore, decreases with the applied strain.

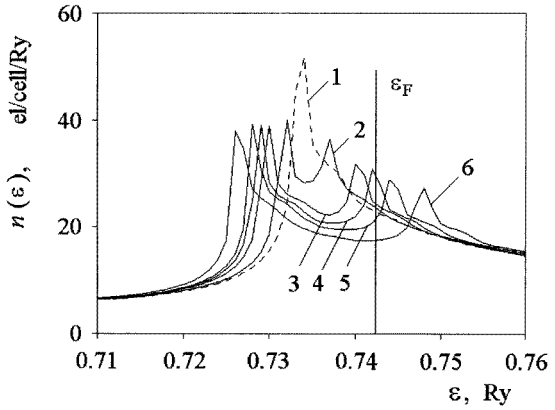

Figure 10. Density of states of the alloy $Ni_{0.625}Al_{0.375}$ under $\Delta = 0.0$ (1), 0.01 (2), 0.02 (3), 0.025 (4), 0.03 (5) and 0.04 (6).

The results under discussion are, again, consistent with the experiment [6]. First, the elevation of the maximum in $\chi(\boldsymbol{q})$ ($\boldsymbol{q} \parallel [110]$) as Δ increases makes intelligible why the dip in the TA$_2$ [110] phonon branch along the same direction deepens. Second, the increasing of the nesting vector $2\boldsymbol{k}_F$ along [110] explains the shifting of the phonon dip to a larger vector (figure 9(a, b)); of course, this fact favours once more the view that the phonon anomaly is none other than a Kohn one. Third, the growth of $\chi(\boldsymbol{q})$ ($\boldsymbol{q} \parallel [110]$) as a whole with the applied stress explains the experimentally observed softening of the entire TA$_2$ [110] curve as it is, again, due to screening via $\chi(\boldsymbol{q})$. The latter is enhanced as the Fermi level ε_F moves towards the higher-energy 2D van Hove singularity, ε_z.

6. Discussion and conclusion

The calculations presented in sections 3, 4 and 5 indicate convincingly that there are two different electronic peculiarities which manifest themselves simultaneously and strongly in the TA$_2$ phonon mode in the β-Ni$_x$Al$_{1-x}$ alloy. One such peculiarity presents the flat pieces of Fermi surface which can be joined by the constant vector $2\boldsymbol{k}_F$; it gives rise to a maximum in the susceptibility function and, correspondingly, to the dip in the TA$_2$ [110] phonon branch. Another electronic feature is the 2D van Hove singularity in the density of states which affects the $\chi(\boldsymbol{q})$ and, therefore, the TA$_2$ phonon branch for all $\boldsymbol{q}$. Of particular interest is a case when uniaxial stress (along [001]) is applied. In this case these two electronic peculiarities manifest themselves in TA$_2$ along the [110]- and $[1, 0, a/c]$-($[0, 1, a/c]$-) directions quite differently.

We do not know any works in which the van Hove singularity effects in the phonon spectrum have been considered for the case of the 2D singularity. At the same time, these effects have been studied quite rigorously for the case of the 3D singularity [20, 21]. Dagens [20] was the first to show that as the Fermi level ε_F approaches the 3D van Hove point ε_C, the phonon frequency squared $\omega^2(\boldsymbol{q})$ gains, in particular, the non-analytical part $\delta\omega^2(\boldsymbol{q}) \approx |\eta|^{3/2}(1 - \theta(\pm\eta))(\eta = \varepsilon_F - \varepsilon_C)$, which exists at one side of the Fermi surface topology change ($\eta \to +0$, or $\eta \to -0$) and for all $\boldsymbol{q}$. Moreover, he has concluded that an average over the phonon spectrum (such as a phonon spectrum moment $\langle\omega^n\rangle$) also has the non-analytical contribution $\sim\eta^{3/2}$ at both sides ($\eta \to \pm 0$). All these results have been

refined by Vaks and Trefilov [21]. First, they found the 'one-sided' anomaly $\delta\omega^2(\boldsymbol{q}) \sim |\eta|^{3/2}$ to be true only for 'large' $q > q_S \sim \eta_\pm^{1/2}$, where $\eta_\pm = \pm\eta\theta(\pm\eta)$. For small $q < q_S$ the anomaly becomes stronger, namely, $\delta\omega^2(\boldsymbol{q}) \propto \eta_\pm^{1/2} q^2$, which is in accordance with the fact that the singular contribution to the elastic moduli $\delta C_{ij} \sim \eta_\pm^{1/2}$ [19]. In the second place, using a simplified exactly soluble model, they, in contrast to Dagens, discovered the phonon average $\langle\omega^n\rangle$ not to contain any singular contributions; this question invites further investigation.

Although the manifestation of the van Hove singularity in the phonon spectrum is not thoroughly clear even for the case of the 3D singularity, we do point out some changes in $\omega(\boldsymbol{q})$ as one goes from the 3D to the 2D singularity. First, the 2D-singularity effects in $\omega^2(\boldsymbol{q})$ are much stronger than those for the 3D one. Indeed, for, say, long waves ($q \sim 0$) the singular part $\delta\omega^2(\boldsymbol{q}) \sim |\eta|^{1/2}$ for the case of the 3D singularity, while for the case of the 2D one it becomes stronger (formally, infinite): $\sim \ln|\eta|$. Such a change is natural: the 2D van Hove singularity can be presented as a great many of the 3D ones merged together. Second, for the case of the 2D singularity the entire phonon dispersion curves gain the critical contribution $\delta\omega^2(\boldsymbol{q}) \sim \delta n(\varepsilon_F)$ along the $\boldsymbol{q}$-lines parallel to those along which the electron bands $\varepsilon_\lambda(\boldsymbol{q})$ have no energy dispersion ($\boldsymbol{V}_\lambda(\boldsymbol{q}) = 0$). For the case of the 3D singularity the similar non-analytical part (proportional to $|\eta|^{1/2}$) holds for all $q > q_S$ and, hence, practically does not depend on q [21]. Finally, we believe that for the case of the 2D singularity a singular contribution to the averages over the phonon spectrum like $\langle\omega^n\rangle$ is distinct from zero. Such a contribution in the case of the 3D singularity, as discussed earlier, seems to be zero [21].

Of course, our analysis of the 2D van Hove singularity effects in the TA_2 phonon branch is only semiqualitative. Further direct first-principles calculations of the lattice dynamics and rigorous analytical consideration are strongly desired here. The Ni–Al alloy system does not provide an exotic example where the effects under discussion are essential. The phonon spectrum of the B2 TiAu-based alloys, for example, also must be strongly influenced by the 2D van Hove singularity—this is seen from the band structures of the TiAu system [22].

Acknowledgments

The research described in this publication was made possible in part by grant no NY7000 from the International Science Foundation and by grant no NY7300 jointly from the International Science Foundation and the Russian Foundation for Basic Research.

References

[1] Pushin V G, Pavlova S P and Yurchenko L I 1989 *Fiz. Met. Metalloved.* **67** 164
[2] Gooding R J and Krumhnsl J A 1989 *Phys. Rev.* B **39** 1535
[3] Shapiro S M, Yang B X, Shirane G, Noda Y and Tanner L E 1990 *Phys. Rev. Lett.* **62** 1298
[4] Noda Y, Shapiro S M, Shirane G, Yamada Y and Tanner L E 1990 *Phys. Rev.* B **42** 10 397
[5] Ye Y Y, Chan C T and Ho K M 1991 *Phys. Rev. Lett.* **66** 2018
[6] Shapiro S M, Svensson E C, Vettier C and Hennion B 1993 *Phys. Rev.* B **48** 13 223
[7] Enami K, Hasuma J, Nagasava A and Nenno S 1976 *Scr. Metall.* **10** 879
[8] Rusovic N and Warlimont H 1977 *Phys. Status Solidi* a **4** 609
[9] Shapiro S M, Larese J Z, Noda Y, Moss S C and Tanner L E 1986 *Phys. Rev. Lett.* **57** 3199
[10] Zhao G L and Harmon B N 1992 *Phys. Rev.* B **42** 2818
[11] Varma C M and Weber W 1979 *Phys. Rev.* B **19** 6142
[12] Naumov I I, Velikokhatny O I and Bashirov V Z 1992 *Sov. Phys.–Solid State* **34** 1790
[13] Anderson O K 1975 *Phys. Rev.* B **12** 3060

[14] Barth U and Hedin L 1972 *J. Phys. C: Solid State Phys.* **5** 1629
[15] Katsnelson M I, Naumov I I and Trefilov A V 1994 *Phase Transitions* **49** 143
[16] Ohta Y and Shimizu M 1983 *J. Phys. F: Met. Phys.* **13** 761
[17] Katsnelson M I, Peschaanskikh G V and Trefilov A V 1990 *Fiz. Tverd. Tela* **32** 470
[18] Rath J and Freeman A J 1975 *Phys. Rev.* B **11** 2109
[19] Vaks V G and Trefilov A V 1988 *J. Phys. F: Met. Phys.* **18** 213
[20] Dagens L 1978 *J. Phys. F: Met. Phys.* **8** 2093
[21] Vaks V G and Trefilov A V 1991 *J. Phys.: Condens. Matter* **3** 1389
[22] Zhang J M and Guo G Y 1995 *J. Phys.: Condens. Matter* **7** 6001